Differential Supercapacitor and Schottky Diode behaviours in Two New Isostructural Coordination Polymers Based on Redox Active Metal Ions

Chhatan Das[a], Subhrajyoti Debnath[b], Vishwas D. Patel[c], Dhritiman Gupta[c], Anjan Banerjee[b*] and Partha Mahata[a*]

[a]Department of Chemistry, Jadavpur University, Kolkata-700032, India. Email: parthachem@gmail.com

[b]Department of Chemistry, Presidency University, 86/1, College Street,Kolkata-700073, West Bengal, India. Email: anjan.chem@presiuniv.ac.in

[c]Department of Physics, School of Advanced Sciences, Vellore Institute of Technology, Vellore 632014, Tamil Nadu, India.

ELECTRONIC SUPPLEMENTARY INFORMATION

*Corresponding Authors, E-mail: parthachem@gmail.com, anjan.chem@presiuniv.ac.in

Table S1: The observed FT-IR bands for $\{[Mn(PDA)(4\text{-bpdb})(H_2O)_2]\cdot 4\text{-bpdb}\}_n$, **1**(Mn) and $\{[Fe(PDA)(4\text{-bpdb})(H_2O)_2]\cdot 4\text{-bpdb}\}_n$, **2**(Fe).

Bands	Absorption Wavenumbers (cm^{-1})	Bands	Absorption Wavenumbers (cm^{-1})
$\upsilon_{str}(H_2O)$	3120(w)	$\upsilon_{sy.\ str}$(carboxylate)	1302(s)
$\upsilon_{asy.str}(sp_2$ C-H)	3052(m), 2924(m)	υ_{str}(C-N)	1230(s), 1195(w)
$\upsilon_{asy.str}(sp_3$ C-H)	2820(w)	δ(aromatic C-H)$_{in}$ plane bending	1156(s), 1063(s), 1018(w),989(m)
$\upsilon_{asy.\ str}$(carboxylate)	1604(s)	δ(aromatic C-H)$_{out}$ of plane bending	944(m), 873(m), 808(w)
υ_{str}(C=N)	1540(s)	$\delta(carboxylate)_{bending}$	717(s), 680(w)
υ_{str}(C=C)	1498(s), 1416(m)	δ(aromatic C=C)$_{out}$ of plane bending	617(s), 512(m)

Table S2: Selected bond distances (Å) observed in {[Mn(PDA)(4-bpdb)(H_2O)$_2$]·4-bpdb}$_n$, **1**(Mn) and {[Fe(PDA)(4-bpdb)(H_2O)$_2$]·4-bpdb}$_n$, **2**(Fe).

1(Mn)		**2** (Fe)	
Bond	Distances, Å	Bond	Distances, Å
Mn(1)-O(1)	2.148(2)	Fe(1)-O(1)	2.1005(18)
Mn(1)-O(1)#1	2.148(2)	Fe(1)-O(1)#1	2.1005(18)
Mn(1)-O(3)	2.215(3)	Fe(1)-O(3)#1	2.172(2)
Mn(1)-O(3)#1	2.215(3)	Fe(1)-O(3)	2.173(2)
Mn(1)-N(1)#1	2.295(3)	Fe(1)-N(1)#1	2.226(2)
Mn(1)-N(1)	2.295(3)	Fe(1)-N(1)	2.226(2)

Symmetry transformations used to generate equivalent atoms: #1 -x+1,-y+1,-z+1.

Table S3: Selected bond angles observed in $\{[Mn(PDA)(4\text{-bpdb})(H_2O)_2]\cdot 4\text{-bpdb}\}_n$, **1**(Mn) and $\{[Fe(PDA)(4\text{-bpdb})(H_2O)_2]\cdot 4\text{-bpdb}\}_n$, **2**(Fe).

Mn(**1**)		Fe(**2**)	
Angle	Amplitude	Angle	Amplitude
O(1)#1-Mn(1)-O(1)	180.0	O(1)-Fe(1)-O(1)#1	180.0
O(1)#1-Mn(1)-O(3)	92.51(10)	O(1)-Fe(1)-O(3)#1	91.31(8)
O(1)-Mn(1)-O(3)	87.49(10)	O(1)#1-Fe(1)-O(3)#1	88.69(8)
O(1)#1-Mn(1)-O(3)#1	87.49(10)	O(1)-Fe(1)-O(3)	88.69(8)
O(1)-Mn(1)-O(3)#1	92.51(10)	O(1)#1-Fe(1)-O(3)	91.31(8)
O(3)-Mn(1)-O(3)#1	180.0	O(3)#1-Fe(1)-O(3)	180.0
O(1)#1-Mn(1)-N(1)#1	87.72(9)	O(1)-Fe(1)-N(1)#1	91.67(7)
O(1)-Mn(1)-N(1)#1	92.28(9)	O(1)#1-Fe(1)-N(1)#1	88.33(7)
O(3)-Mn(1)-N(1)#1	88.48(10)	O(3)#1-Fe(1)-N(1)#1	90.32(8)
O(3)#1-Mn(1)-N(1)#1	91.52(10)	O(3)-Fe(1)-N(1)#1	89.68(8)
O(1)#1-Mn(1)-N(1)	92.28(9)	O(1)-Fe(1)-N(1)	88.33(7)
O(1)-Mn(1)-N(1)	87.73(9)	O(1)#1-Fe(1)-N(1)	91.67(7)
O(3)-Mn(1)-N(1)	91.52(10)	O(3)#1-Fe(1)-N(1)	89.68(8)
O(3)#1-Mn(1)-N(1)	88.48(10)	O(3)-Fe(1)-N(1)	90.32(8)
N(1)#1-Mn(1)-N(1)	180.0	N(1)#1-Fe(1)-N(1)	180.0

Symmetry transformations used to generate equivalent atoms: #1 -x+1,-y+1,-z+1.

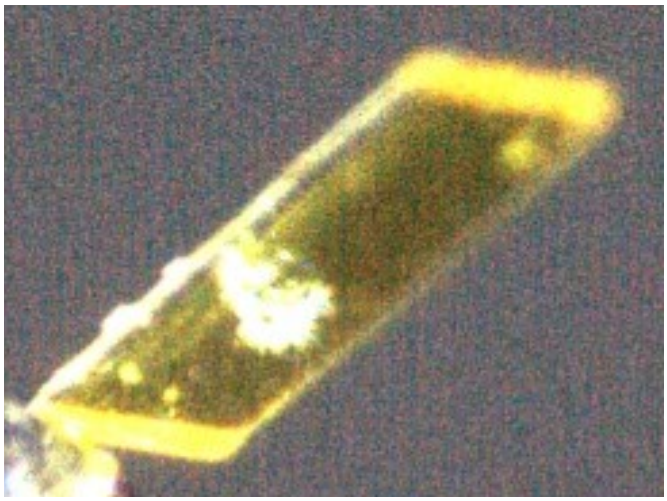

Fig. S1a: Yellow coloured parallelogram shaped crystal structure of {[Mn(PDA)(4-bpdb)$(H_2O)_2$]·4-bpdb}$_n$, **1**(Mn).

Fig. S1b: Violet coloured parallelogram shaped crystal image of {[Fe(PDA)(4-bpdb)$(H_2O)_2$]·4-bpdb}$_n$, **2**(Fe).

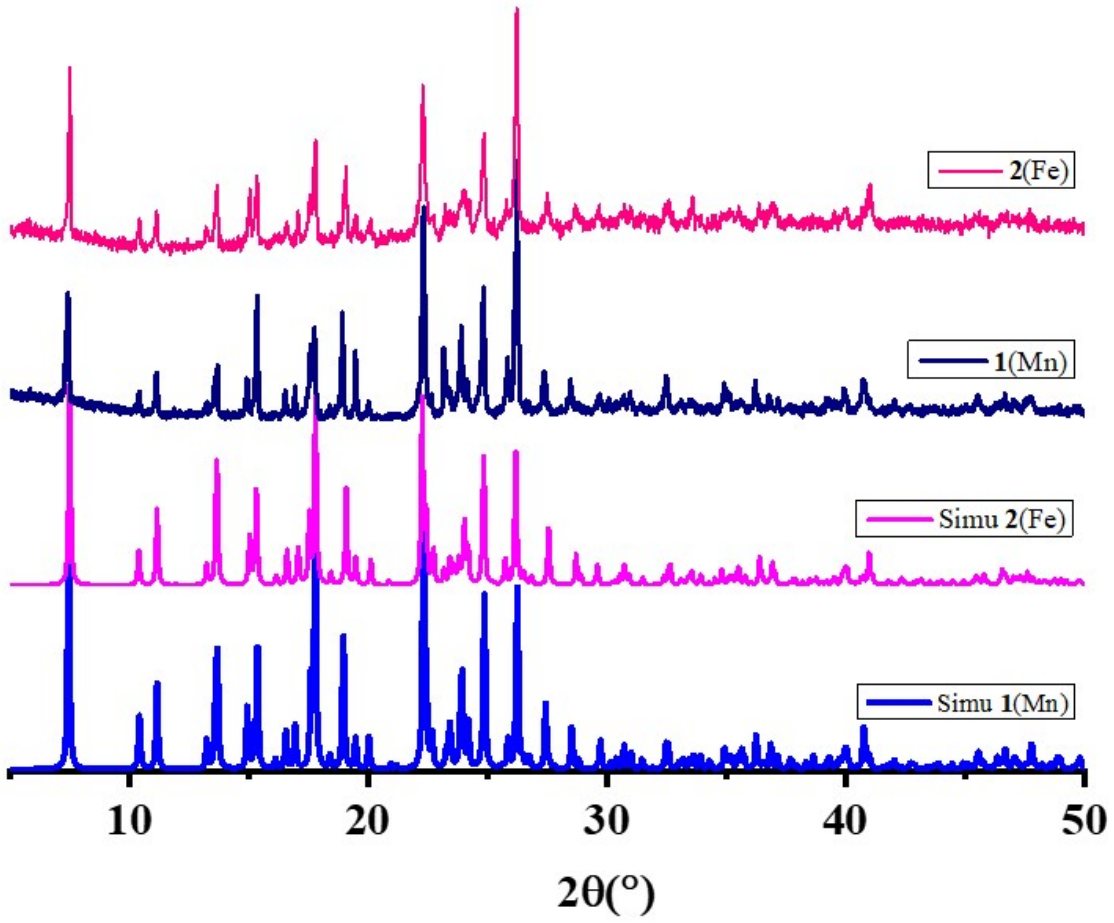

Fig. S2: PXRD (CuKα) patterns of $\{[Mn(PDA)(4\text{-bpdb})(H_2O)_2]\cdot 4\text{-bpdb}\}_n$, **1**(Mn) and $\{[Fe(PDA)(4\text{-bpdb})(H_2O)_2]\cdot 4\text{-bpdb}\}_n$, **2**(Fe).

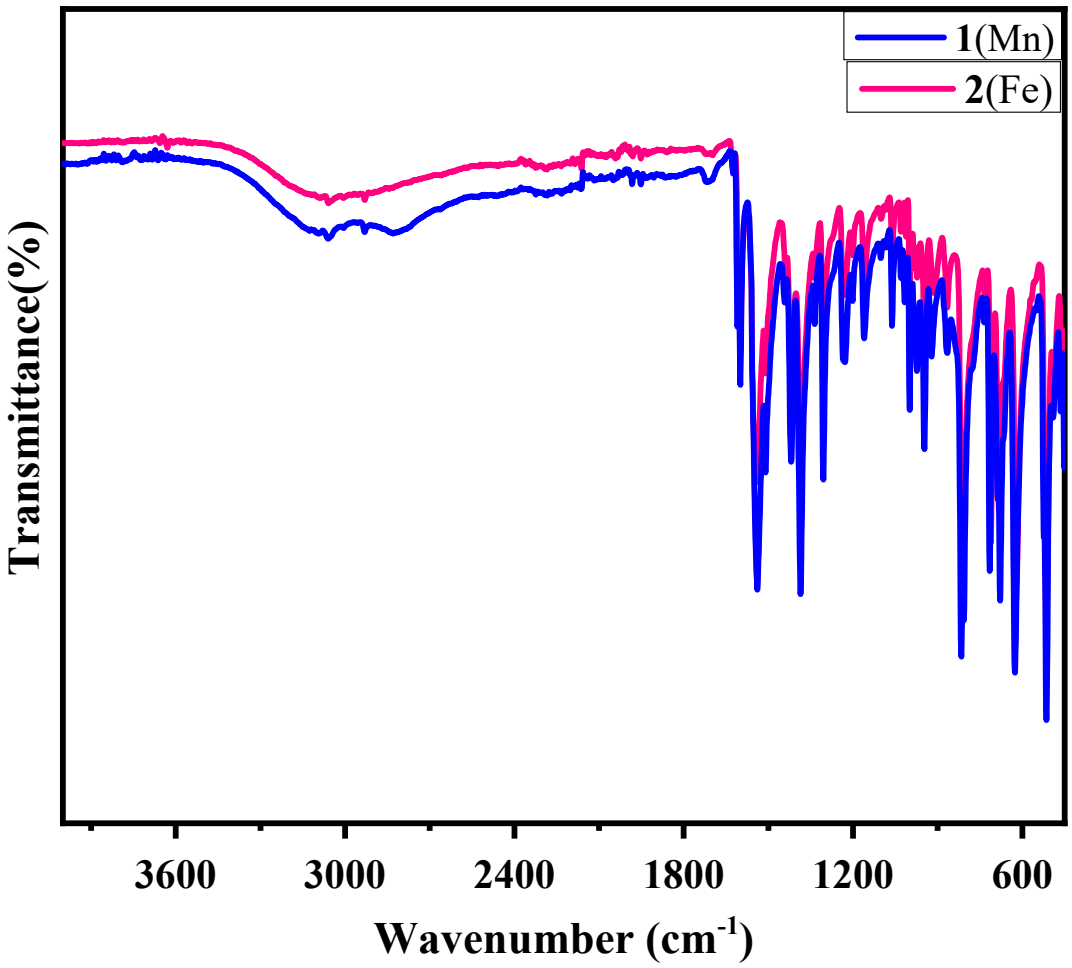

Fig. S3: FT-IR spectrum of {[Mn(PDA)(4-bpdb)(H_2O)$_2$]·4-bpdb}$_n$, **1**(Mn) and {[Fe(PDA)(4-bpdb)(H_2O)$_2$]·4-bpdb}$_n$, **2**(Fe).

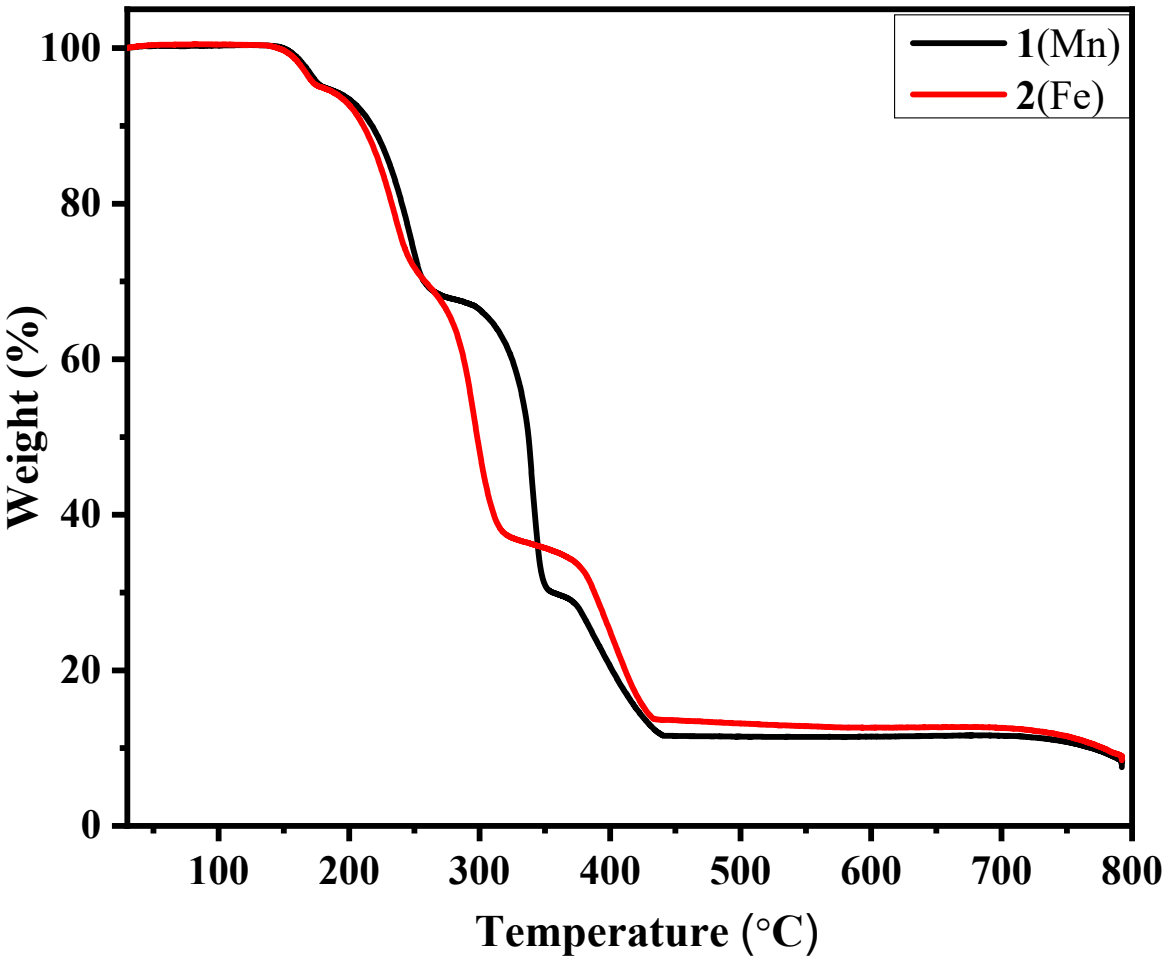

Fig. S4: Thermogravimetric analysis (TGA) of $\{[Mn(PDA)(4\text{-bpdb})(H_2O)_2]\cdot 4\text{-bpdb}\}_n$, **1**(Mn) and $\{[Fe(PDA)(4\text{-bpdb})(H_2O)_2]\cdot 4\text{-bpdb}\}_n$, **2**(Fe) in nitrogen atmosphere.

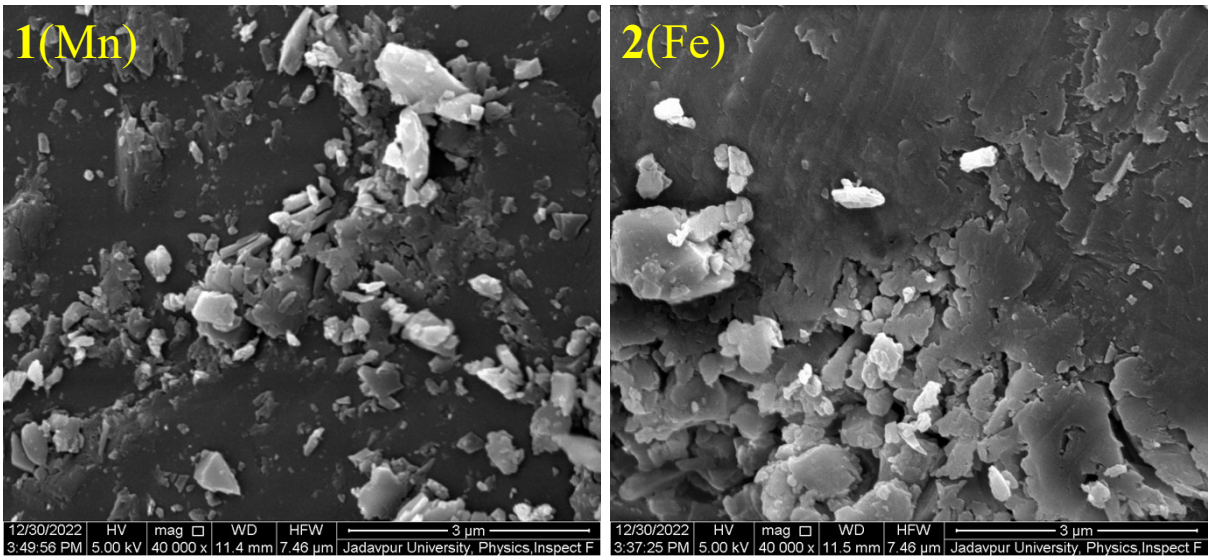

Figure S5: SEM images of $\{[Mn(PDA)(4\text{-bpdb})(H_2O)_2]\cdot 4\text{-bpdb}\}_n$, **1**(Mn) and $\{[Fe(PDA)(4\text{-bpdb})(H_2O)_2]\cdot 4\text{-bpdb}\}_n$, **2**(Fe).

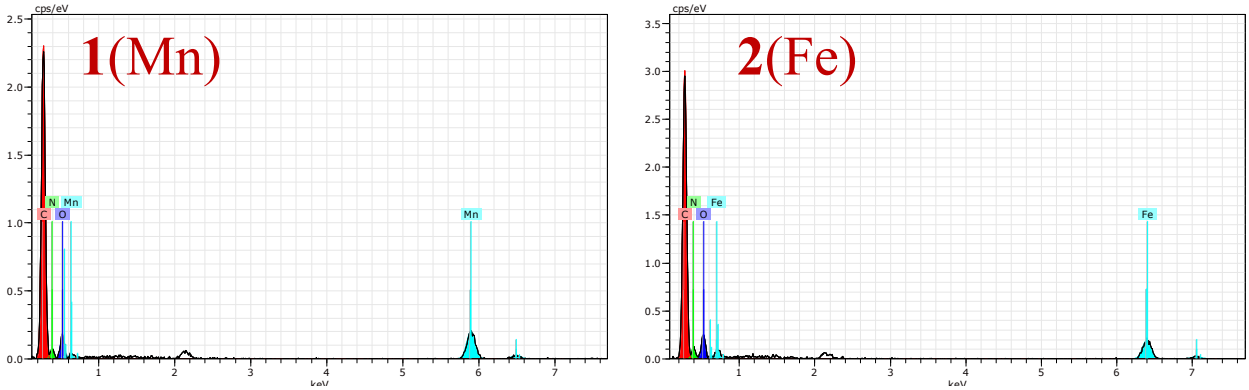

Figure S6: Representative EDX plot of $\{[Mn(PDA)(4\text{-bpdb})(H_2O)_2]\cdot 4\text{-bpdb}\}_n$, **1**(Mn) and $\{[Fe(PDA)(4\text{-bpdb})(H_2O)_2]\cdot 4\text{-bpdb}\}_n$, **2**(Fe). Note the presence of Mn and Fe.

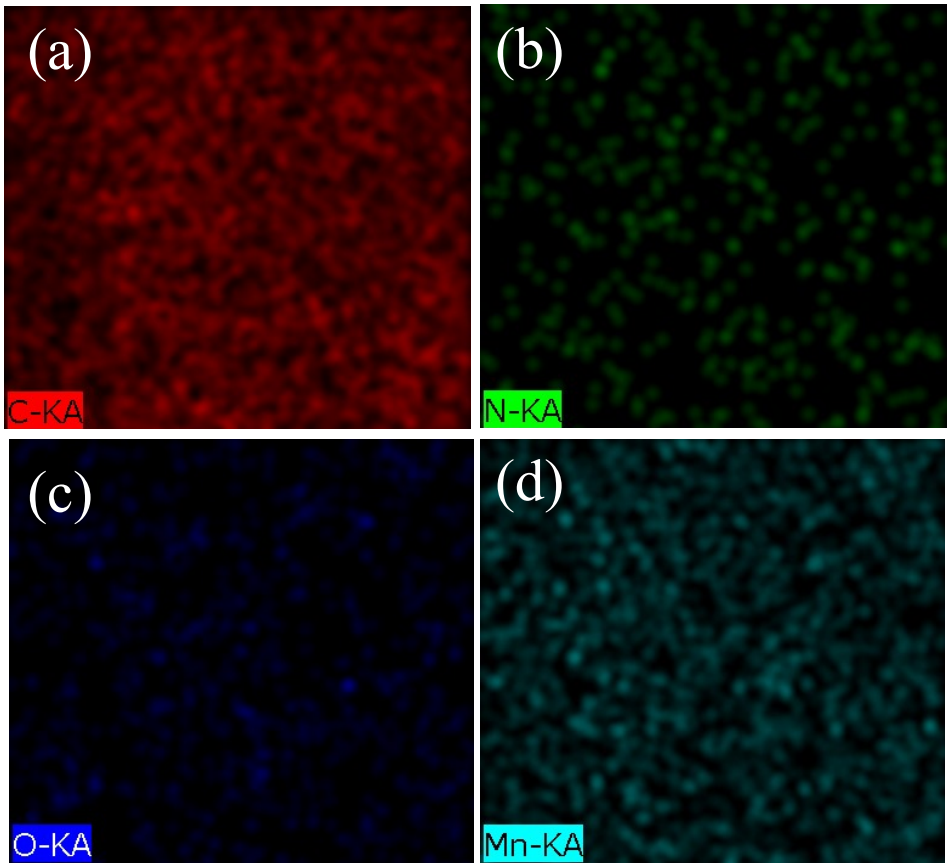

Figure S7**.** Elemental mapping images of $\{[Mn(PDA)(4\text{-bpdb})(H_2O)_2]\cdot 4\text{-bpdb}\}_n$, **1**(Mn) for (a) C-KA and (b) N-KA, (c) O-KA and (d) Mn-KA.

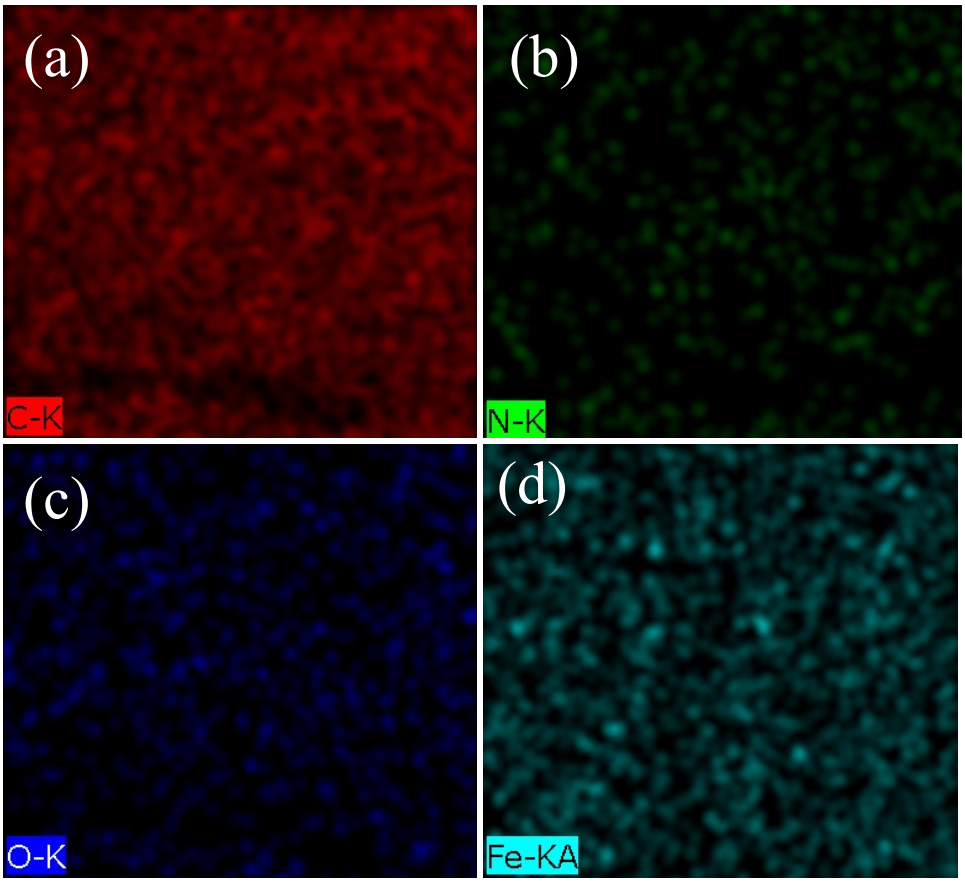

Figure S8**.** Elemental mapping images of {[Fe(PDA)(4-bpdb)(H_2O)$_2$]·4-bpdb}$_n$, **2**(Fe) for (a) C-K and (b) N-K, (c) O-K and (d) Fe-KA.

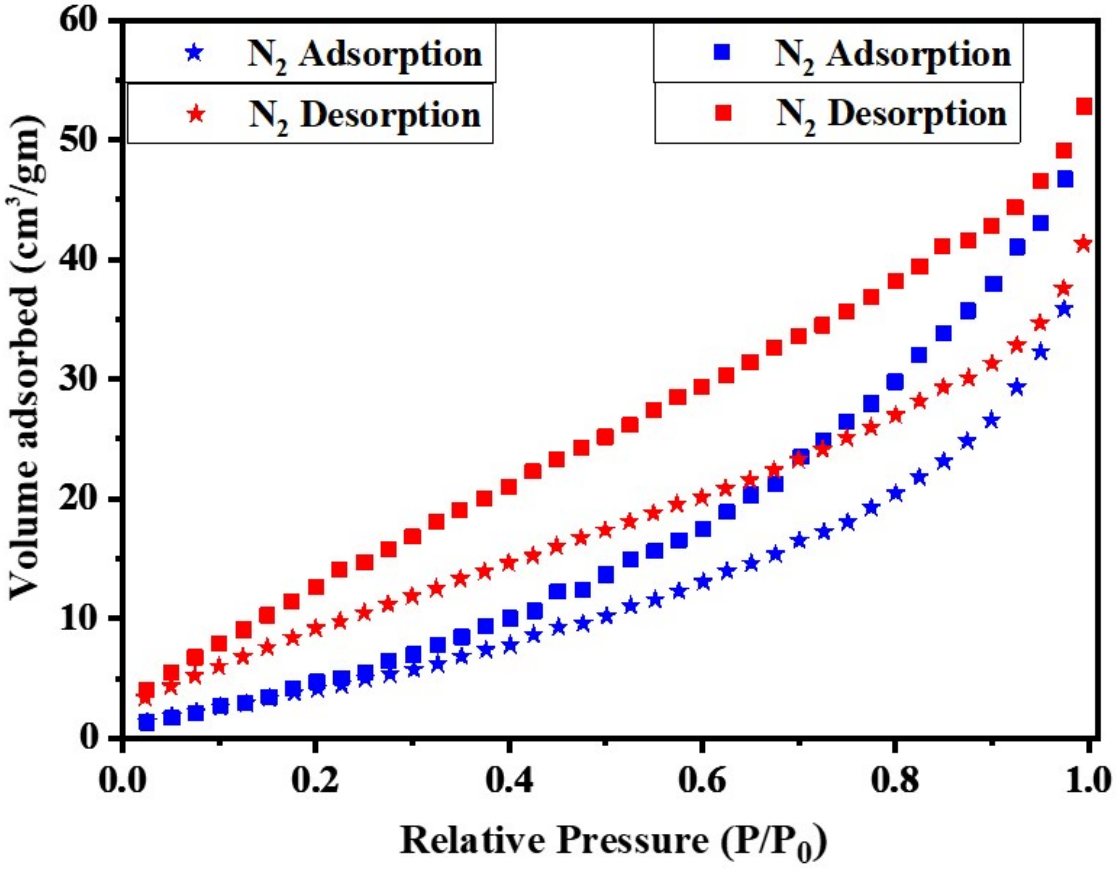

Fig. S9: N_2 adsorption (at 77 K) isotherms of **1**(Mn**)** and **2**(Fe), squares represent the adsorption(blue) and desorption(red) by **1**(Mn) and stars represent the adsorption(blue) and desorption(red) by **2**(Fe), respectively.

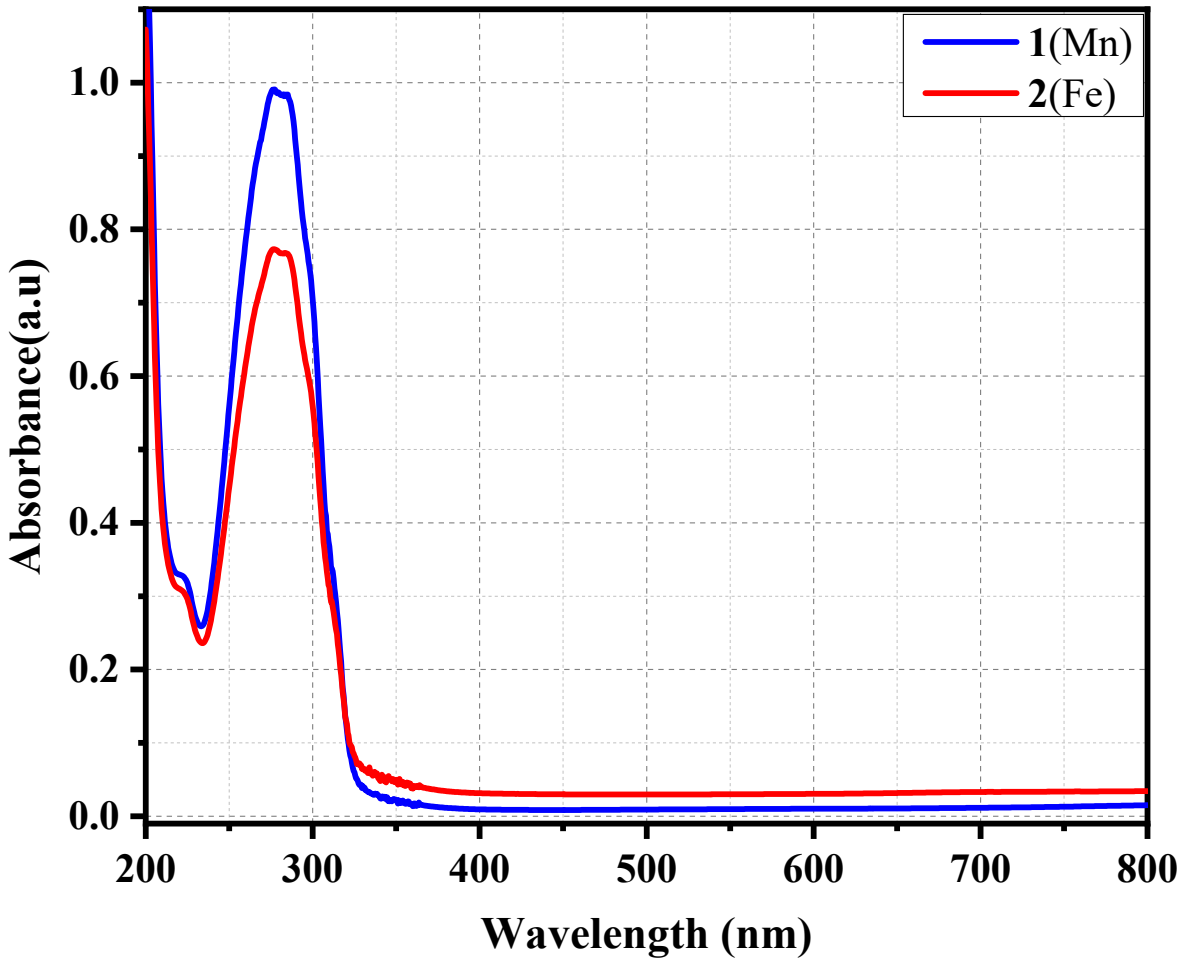

Fig. S10: Absorption spectra of **1**(Mn) and **2**(Fe) in aqueous medium.

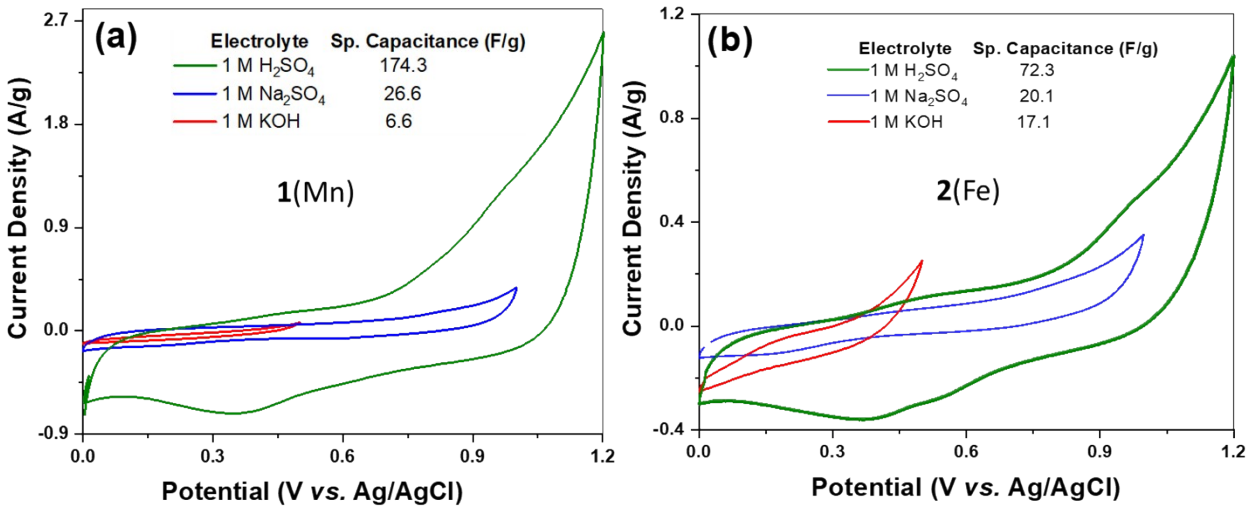

Fig. S11: Comparative CV profiles of (a) **1**(Mn) and (b) **2**(Fe) at 5 mV/s scan rate under 1 M H_2SO_4, 1 M Na_2SO_4 and 1 M KOH electrolyte mediums.

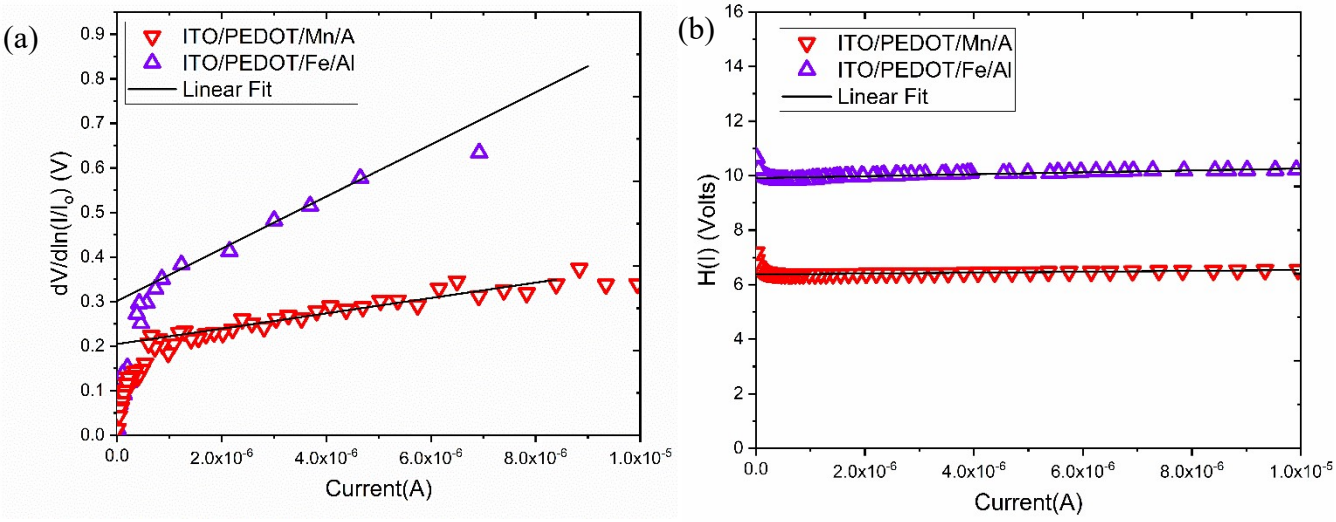

Fig. S12: (a)*Plot of* $dV \Big/ d\ln\left(\frac{I}{I_0}\right)$ *versus I and (b) H(I) vs. I for the devices ITO/PEDOT/Fe/Al and ITO/PEDOT/Mn/Al in dark condition*

Table S4

Device Structure	Series resistance R_s (KΩ)		Ideality factor (n)	Barrier height φ_B (eV)
	From $dV \Big/ d\left(\ln\frac{I}{I_0}\right)$ vs I	From $H(I)$ vs I		
ITO/PEDOT/Mn/Al	17.22 ± 1.22	16.60 ± 0.5	7.75	0.821
ITO/PEDOT/Fe/Al	58.51 ± 4.04	34.99 ± 1.50	11.66	0.849